Int. J. Heat Mass Transfer. Vol. 27, No. 2, pp. 191–205, 1984
Printed in Great Britain

0017-9310/84 $3.00 + 0.00

CONVECTIVE AND RADIATIVE HEATING OF A SATURN ENTRY PROBE

S. N. Tiwari,† K. Y. Szema,‡ J. N. Moss§ and S. V. Subramanian‖

† School of Engineering, Old Dominion University, Norfolk, VA 23508, U.S.A.; † Rockwell International Corporation, Thousand Oaks, CA 91360, U.S.A.; § NASA Langley Research Center, Hampton, VA 23665, U.S.A.; ‖ AVCO-LYCOMING, Stratford, CT 06497, U.S.A.

(*Received* 23 *August* 1982 *and in revised form* 22 *April* 1983)

Abstract—The extent of convective and radiative heating for a Saturn entry probe is investigated in the absence and presence of ablation mass injection. The flow in the shock layer is assumed to be axisymmetric, viscous and in local thermodynamic equilibrium. The importance of chemical nonequilibrium effects for both the radiative and convective nonblowing surface heating rates is demonstrated for prescribed entry conditions. Results indicate that the nonequilibrium chemistry can significantly influence the rate of radiative heating to the entry probes. With coupled carbon–phenolic ablation injection, the convective heating rates are reduced substantially. Turbulence has little effect on radiative heating but it increases the convective heating considerably.

NOMENCLATURE

C_i	mass fraction of species i in the shock layer, ρ_i/ρ
C_p	equilibrium specific heat of mixture, $\Sigma C_i C_{p,i}$
$C_{p,i}$	specific heat of species i, $C^*_{p,i}/C^*_{p,\infty}$
D_{ij}	binary diffusion coefficient
h	specific enthalpy, h^*/V^{*2}_∞
H	total enthalpy, $h+u^2/2$ (also atomic hydrogen)
H^+	hydrogen ions
J_i	mass diffusion flux of species i, $J^*_i R_N/\mu^*_{ref}$
k	thermal conductivity of mixture, $k^*/\mu^*_{ref}C^*_{p,\infty}$ (also Boltzmann constant)
K^*_α	net rate of production of species α
Le	Lewis number, $\rho^* D^*_{ij} C^*_p/k^*$
M^*	molecular weight of mixture
n	coordinate normal to the bow shock, n^*/R^*_N
p	pressure, $p^*/(\rho^*_\infty V^{*2}_\infty)$
Pr	Prandtl number, $\mu^* C^*_p/k^*$
q_R	net radiant heat flux, $q^*_R/(\rho^*_\infty V^{*3}_\infty)$
r	radius measured from axis of symmetry to a point on the body surface, r^*/R^*_N
R^*	universal gas constant
R^*_b	radius of the body
R^*_N	body nose radius (same as R^*_n)
R^*_s	radius of the bow shock
T	temperature, T^*/T^*_{ref}
T^*_{ref}	reference temperature, $V^{*2}_\infty/C^*_{p,\infty}$
u	velocity tangent to body surface, u^*/V^*_∞
v	velocity normal to body surface, v^*/V^*_∞
x	coordinate along the body surface, x^*/R^*_N
y	coordinate normal to the body surface, y^*/R^*_N.

Greek symbols

α	shock angle defined in Fig. 1
ε	Reynolds number parameter
θ	body angle defined in Fig. 1
η	transformed y-coordinate, y/y_s
κ	body curvature, $\kappa^* R^*_N$
κ_ν	special absorption coefficient
μ	viscosity of mixture, μ^*/μ^*_{ref}
μ^*_{ref}	reference viscosity, $\mu^*(T^*_{ref})$
ξ	coordinate along the body surface, x
ρ	density of mixture, ρ^*/ρ^*_∞
τ	optical coordinate
τ_0	optical coordinate.

Subscripts

i	ith species
s	shock value
w	wall value
∞	freestream condition
ν	radiation frequency.

INTRODUCTION

The recent planetary exploration program of the National Aeronautics and Space Administration includes the Mars Surface Sample Return (MSSR), Saturn Orbiter Dual Probe (SO2P), and Titan Orbiter (TO) missions. For the SO2P mission, it is proposed to use much of the software technology and probe design developed for the Project Galileo ıor entry into Jupiter's atmosphere. The aerothermal environment of a Saturn entry probe can, therefore, be investigated by extending the existing analyses to the trajectories proposed for the Saturn mission [1].

The influence of chemical nonequilibrium (in the shock-layer gas) on the entire flow phenomena around a Jovian entry body has been investigated recently [2, 3]. It was found that inclusion of the nonequilibrium chemistry in the viscous-shock-layer (VSL) analysis increases the radiative heating rates to the entry body significantly. The effect of nonequilibrium was found to be particularly important at high altitude (higher entry velocities) entry conditions. Through an entirely different species concentration and temperature

distribution, the nonequilibrium chemistry of the shock-layer gas was found to affect the entire flow field around the entry probe. It was concluded that inclusion of the nonequilibrium gas chemistry is essential in the study of the aerothermal environment of the outer-planetary entry vehicles.

The aerothermal environment of a Saturn entry probe has been investigated in a few preliminary studies [4–8]. The effect of nonequilibrium chemistry, however, was not considered in a rigorous VSL analysis. At certain entry conditions [1], this could have a significant influence on the entire flow field around the entry probe. In certain analyses it is convenient to use the approximate equation of state, approximate radiation models, and simple relations for thermodynamic and transport properties [2, 8, 9]. While such relations are useful for general parametric studies, they may lead to significant errors in specific cases [10]. At present, certain uncertainties also exist on the extent of laminar and turbulent heating (convective as well as radiative) rates to the Saturn entry probe in the presence of ablation mass injection [8, 10].

The purpose of this study is to investigate the aerothermal environment of a Saturn entry probe for different flow conditions and determine the extent of convective and radiative heatings for the currently specified entry trajectories. The VSL analyses used for the Galileo probe design [2, 11–15] are employed (with appropriate modifications) in this study also. The entry bodies considered are a 35° hyperboloid and a 45° sphere cone at 0° angle of attack. The nominal composition of Saturn's atmosphere is assumed to consist of 89% H_2 and 11% He by volume [6]. For sake of computational convenience, the effect of chemical nonequilibrium is investigated only for the case of laminar flow with no mass injection. Laminar and turbulent flow results (with and without mass ablation) are compared for peak heating conditions. Although the results obtained in this study are for specific Saturn entry conditions, the entire analysis can be applied to other planetary entry conditions for general parametric studies [17].

ANALYSIS

The entry bodies considered for this study are a 35° hyperboloid and a 45° sphere cone (the proposed baseline configuration for the Saturn entry probe) at an angle of attack of 0°. The 35° sphere cone, is considered for the sake of comparison and convenience.

The physical model and coordinate system for a Saturn entry body are shown in Fig. 1. The flow in the shock layer is assumed to be axisymmetric, steady, viscous, and compressible. The shock-layer gas is assumed to be in local thermodynamic equilibrium. The general equations of motions for reacting gas mixtures are available in refs. [18–20]. The formulations of these equations in body oriented coordinates appropriate for viscous-shock-layer analyses of

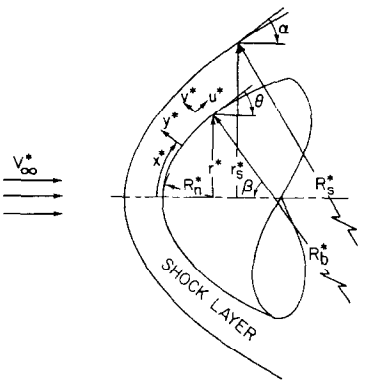

FIG. 1. Physical model and coordinate system.

radiating gases are presented in refs. [11, 12, 21]. The governing equations for the present physical model are similar to those given in refs. [2, 11, 21] and, therefore, only the basic equations applicable to this study are presented here.

Governing equations

The viscous-shock-layer equations are obtained from the steady-state Navier–Stokes equations by retaining terms up to second order in the inverse square root of the Reynolds number. The set of governing equations appropriate for this study is expressed as [2, 11]:

continuity

$$(\partial/\partial x)[(r+y\cos\theta)\rho u]+(\partial/\partial y)(\Gamma\zeta\rho v)=0, \quad (1)$$

x momentum

$$\rho[(u/\Gamma)(\partial u/\partial x)+v(\partial u/\partial y)+uv\kappa/\Gamma]+\Gamma^{-1}(\partial p/\partial x)$$
$$=\varepsilon^2[(\partial/\partial y)(\mu\psi)+\mu(2\kappa/\Gamma+\cos\theta/\zeta)\psi], \quad (2)$$

y momentum

$$\rho[(u/\Gamma)(\partial v/\partial x)+v(\partial v/\partial y)-u^2\kappa/\Gamma+\partial p/\partial y=0, \quad (3)$$

energy

$$\rho[(u/\Gamma)(\partial H/\partial x)+v(\partial H/\partial y)]-v(\partial p/\partial y)+\rho\kappa u^2 v/\Gamma$$
$$=\varepsilon^2[\partial\phi/\partial y+(\kappa/\Gamma+\cos\theta/\zeta)\phi]-\operatorname{div} q_r, \quad (4)$$

species continuity

$$\rho[(u/\Gamma)(\partial C_i/\partial x)+v(\partial C_i/\partial y)]$$
$$=\dot{w}_i-(\varepsilon^2/\Gamma\zeta)[(\partial/\partial y)(\Gamma\zeta J_i)], \quad (5)$$

where

$$\Gamma=1+y\kappa, \quad \zeta=r+y\cos\theta, \quad (6a)$$

$$\varepsilon=[\mu^*_{\mathrm{ref}}/(\rho^*_\infty V^*_\infty R^*_N)]^{1/2}, \quad \psi=\partial u/\partial y-u\kappa/\Gamma, \quad (6b)$$

$$\phi=\frac{\mu}{Pr}\left[\frac{\partial H}{\partial y}-\sum_{i=1}^{N}h_i\frac{\partial C_i}{\partial y}-\frac{Pr}{\mu}\sum_{i=1}^{N}\times h_i J_i+(Pr-1)\mu\frac{\partial u}{\partial y}-Pr\,\kappa\frac{u^2}{\Gamma}\right], \quad (6c)$$

$$H=h+u^2/2, \quad J_i=(\mu/Pr)Le(\partial C_i/\partial y). \quad (6d)$$

In equation (5), $\dot{w}_i$ represents the rate of production of the chemical species in the shock layer and is given by the relation

$$\dot{w}_i = M_i^*(\mathrm{d}x_i/\mathrm{d}t)(R_N^*/\rho_\infty^* V_\infty^*), \tag{7}$$

where x_i represents the mole fraction of species i. Complete information on chemical reactions, rate constants, and electron temperature is given in ref. [2].

For the case of chemical equilibrium, it is convenient to use the elemental continuity equation instead of the species continuity equation because elemental mass fractions remain fixed during chemical reactions. The relation between the elemental and species mass fraction is given by

$$C_l = \sum_{i=1}^{N} \delta_{il}(M_l^*/M_i^*)C_i. \tag{8}$$

The elemental continuity equations can be obtained by multiplying equation (5) by $\delta_{il}(M_l^* C_i/M_i^*)$ and summing over i; this results in

$$\rho[(u/\Gamma)(\partial C_l/\partial x)+v(\partial C_l/\partial y)] = -(\varepsilon^2/\Gamma\zeta)[(\partial/\partial y)(\Gamma\zeta J_l)], \tag{9}$$

where

$$J_l = \sum_{i=1}^{N} \delta_{il}(M_l^*/M_i^*)J_i.$$

For equilibrium flow, therefore, equation (5) is replaced by equation (9) and this reduces the number of equations to be solved.

For the equilibrium case, the equation of state, in general, is given by

$$P = \rho T R^*/\bar{M}^* C_{p,\infty}^*. \tag{10}$$

This is an exact equation of state for the equilibrium case. Certain computational conveniences are realized by employing approximate equations of state for equilibrium flows. For a hydrogen/helium mixture, approximate expressions for the equations of state are given by Zoby *et al.* [22] as

$$T^* = C_T[(p^*/1\,013\,250)^l/(\rho^* 10.001292)^k], \tag{11a}$$

$$H^* = C_H[(p^*/1\,013\,250)^m/(\rho^* 10.001292)^n] \times (R^* T_0^*/M^*), \tag{11b}$$

where

$$C_T = C_T(U_t)+61.2(1-x_{H_2}),$$

$$C_H = C_H(U_t)-0.3167(1-x_{H_2}).$$

In this equation, x_{H_2} represents the mole fraction of H_2, and values of quantities k, l, m, n, $C_T(U_t)$, and $C_H(U_t)$ are given in refs. [2, 22].

For the condition of chemical nonequilibrium, the basic governing equations are essentially the same as for the equilibrium condition with exception of the species production term $\dot{w}_i$ in equation (5). However, the exact equation of state for the nonequilibrium case is given by the relation [2, 20]

$$p^* V^* = \sum_i (N_i) R^* T^*, \tag{12}$$

where N_i is the number of moles for the ith species.

The set of governing equations presented previously have a hyperbolic–parabolic nature. The hyperbolic nature enters through the normal momentum equation. If the shock layer is assumed to be thin, then the normal momentum equation can be expressed as

$$\rho u^2 \kappa/(1+y\kappa) = \partial p/\partial y. \tag{13}$$

If equation (3) is replaced with equation (13), then the resulting set of equations is parabolic. These equations can, therefore, be solved by using numerical procedures similar to those used in solving boundary-layer problems [11, 23].

The basic governing equations, equations (1)–(9), can be modified to apply to turbulent flows by introducing the eddy-viscosity approximation. Complete information on the turbulence model and an appropriate governing equation is available in refs. [15, 21]. The difference in the laminar and turbulent flow equations lies in the definitions of ψ, ϕ, and J_i. For turbulent flow, these are defined as

$$\psi = (1+\varepsilon^+)\,\partial u/\partial y - \mu\kappa/\Gamma, \tag{14a}$$

$$\phi = \phi_1 + \phi_2 + \phi_3, \tag{14b}$$

$$\phi_1 = (\mu/Pr)[1+\varepsilon^+(Pr/Pr_t)](\partial H/\partial y), \tag{14c}$$

$$\phi_2 = (\mu/Pr)[Pr-1+\varepsilon^+(Pr/Pr_t)(Pr_t-1)] \times u(\partial u/\partial y)-\mu\kappa u^2/\Gamma, \tag{14d}$$

$$\phi_3 = (\mu/Pr)[Le-1+\varepsilon^+(Pr/Pr_t)(Le_t-1)] \times \sum_{i=1}^{N} h_i(\partial C_i/\partial y), \tag{14e}$$

$$J_i = (\mu/Pr)[Le+\varepsilon^+(Pr/Pr_t)Le_t](\partial C_i/\partial y). \tag{14f}$$

Note that for $\varepsilon^+ = 0$, the above definitions of ψ, ϕ, and J_i reduce to the case of laminar flow.

Boundary conditions

In order to solve the preceding set of governing equations, it is essential to specify appropriate boundary conditions at the body surface and the shock. For the case with no mass ablation (i.e. $\dot{m} = 0$), no-slip and no-temperature jump conditions are used at the body surface (wall). Thus, $u_w = v_w = 0$, and the wall temperature is specified as $T_w = 4000$ K for all cases considered in this study for $\dot{m} = 0$. Furthermore, it is assumed that the chemical species are in equilibrium at the body surface. The conditions immediately behind the shock are obtained by using the Rankine–Hugoniot relations under the assumption that the gas is frozen across the shock.

For the calculated mass injection conditions, the ablation process is assumed to be quasi-steady and the wall temperature is taken to be the sublimation temperature of the ablator surface. Under these

conditions, the relation for the coupled mass injection rate is given by [12–15]

$$\dot{m} = [-(q_{c,w}+q_{r,w})/SUM](1/\rho_\infty^* V_\infty^*), \quad (15)$$

where

$$SUM = \sum_{i=1}^{N} (C_i h_i^*)_w - h_A^*.$$

The sublimation temperature calculated for the carbon–phenolic ablator considered in this study is

$$T_{sub}^* = 3990 + 340 \log p_w^* - 10(\log p_w^*)\,[\mathrm{K}], \quad (16)$$

where p_w^* is the wall pressure in atmospheres. The coupled mass injection rate and surface temperature are calculated by iterating the solution of the governing flow-field equations and the boundary conditions.

For ablation injection, the elemental concentrations at the wall are governed by convection and diffusion and is given by the relation

$$(\partial C_l/\partial y)_w - \varepsilon^{-2}(\dot{m}\,Sc/\mu)_w[(C_l)_w - (C_l)_-] = 0. \quad (17)$$

The heat transferred to the wall due to conduction and diffusion is referred to as the convective heat flux and is given by the relation

$$q_c = q_{c,w} = -\varepsilon^{-2}\left[k(\partial T/\partial y) + (\mu/Sc)\sum_{i=1}^{N}(\partial C_i/\partial y)h_i\right]_w. \quad (18)$$

For this study, the bow shock is considered transparent, and the free stream is considered cold and transparent; also, the body surface is assumed to be nonreflecting and gray. Consequently, in radiative transport calculations, the precursor effects are neglected but the energy reradiated from the surface is included. For a nonreflecting gray surface, the radiative flux from the surface is given by

$$q_{r,w}^* = \varepsilon_w \sigma^* T_w^{*4}. \quad (19)$$

In this study, the value of the surface emittance ε_w is assumed to be 0.8.

Radiation transport model

The radiative heat flux is calculated with the assumption of a non-scattering medium, the tangent slab approximation for the radiative transfer, and nonreflecting bounding surfaces. The tangent slab approximation implies that the radiative energy transfer along the body is negligible in comparison to that transferred in the direction normal to the body. It should be noted that the tangent slab approximation is used only for the radiative transport and not for other flow variables. For this physical model, the expression for net radiative flux in the shock layer is given by [2, 24]

$$q_r = q_r^+ - q_r^-, \quad (20)$$

where q_r^+ represents the energy transfer towards the shock and q_r^- the energy transfer towards the body. Complete formulations for q_r^+ and q_r^- are available in the cited references; the simplified relations applicable to the present study are

$$q_r^+ = 2\pi\int_0^\infty \left[\varepsilon_{1\nu} B_\nu(T_w)E_3(\tau_\nu) + \int_0^{\tau_\nu} B_\nu(t)E_2(\tau_\nu - t)\,dt\right]d\nu, \quad (21a)$$

$$q_r^- = 2\pi\int_0^\infty \left[\varepsilon_{2\nu} B_\nu(T_s)E_3(\tau_{0\nu} - \tau_\nu) + \int_{\tau_\nu}^{\tau_{0\nu}} B(t)E_2(t - \tau_\nu)\,dt\right]d\nu. \quad (21b)$$

In the preceding equations, $B_\nu(T)$ represents the Planck function, $E_n(t)$ is the exponential integral function of order n, $\varepsilon_{1\nu} = \varepsilon_w$ is the surface emittance, and $\varepsilon_{2\nu}$ represents the emittance of the shock, which is taken to be zero. The quantities τ_ν and $\tau_{0\nu}$ represent the optical coordinate and optical thickness, respectively, and are defined in refs. [2, 24].

Two different models are used to calculate the radiative flux q_r. For the shock-layer gas, a 58-step absorption model as suggested in ref. [9] gives accurate results in comparison to the detailed radiation models [25, 26]. For the case with no mass injection, equilibrium as well as nonequilibrium results are obtained by using this approximate radiation model. For nonequilibrium analysis, the radiative flux is calculated by using the nonequilibrium species concentration and an effective electronic temperature [2]. Equilibrium results are obtained also by employing a detailed radiation code RAD [26, 27]. This code accounts for detailed nongray radiation absorption and emission processes and is used to calculate radiative flux in the presence of mass injection. The chemical species considered for determining the radiative transport are H, H_2, H^+, e^-, C, C_2, C_3, C^+, C^-, CO, O, O_2, O^+, and O^-. The radiation properties used for C_2 and C_3 are those reported in refs. [28, 29].

Eddy-viscosity approximation

A two-layer eddy-viscosity model consisting of an inner law based upon Prandtl's mixing-length concept and the Clauser–Klebanoff expression for the outer law [30, 31] is used in this study. This model, introduced by Cebeci [32], assumes that the inner law is applicable to the flow from the wall out to the location where the eddy-viscosity given by the inner law is equal to that of the outer law. The outer law is then assumed applicable for the remainder of the viscous layer. It is noted that the eddy-viscosity degenerates to approximately zero in the inviscid portion of the shock layer. The degeneracy is expressed in terms of the normal intermittency factor given by Klebanoff [31].

For this study, the boundary-layer edge location, δ, is defined by an index of dissipation expressed as

$$\left\{\int_0^\delta [\tau^2/\mu(1+\varepsilon^+)]\,dy\right\} \Big/ \left\{\int_0^{y_s} [\tau^2/\mu(1+\varepsilon^+)]\,dy\right\} = 0.95, \quad (22)$$

where τ is the local shear stress.

The turbulent Prandtl and Lewis numbers are assumed to be 0.9 and 1.0, respectively. Further information on the turbulence relations used in this study is available in refs. [15, 21].

PHYSICAL CONDITIONS AND DATA SOURCE

The nose radius for both entry body configurations (35° hyperboloid and 45° sphere cone) is taken to be $R_N^* = 0.3112$ m and $R_B^*/R_N^* = 2.0$. For the case with ablation injection, the ablative material considered is carbon–phenolic with 92% carbon, 6% oxygen, and 2% hydrogen by mass. The body surface temperature is taken to be uniform at 4000 K for the case with no injection. For the injection case, however, the surface temperature is the sublimation temperature of the ablator.

Chemical composition of gas mixture

Analyses of chemically reacting flows are usually simplified by assuming a chemical equilibrium behavior of the gas mixture. While this assumption may be justified in many cases, in some realistic problems this may lead to serious errors. Thus, in order to understand the degree of physical reality, it becomes essential to analyze the complex gas mixture under the conditions of chemical nonequilibrium. Complete information on chemical equilibrium and nonequilibrium reactions and reaction rates for the shock-layer gas mixture is given in ref. [2] for Jovian entry conditions. The same basic information is used also for the Saturn entry conditions. For equilibrium case, the number density of eight chemical species (H_2, H, H^+, H^-, e^-, He^-, and He^{2+}) are calculated by the chemical reactions and rate constants given in ref. [9]. For the nonequilibrium case, the finite rate chemistry model based on the Leibowitz and Kuo [6] formulation is used to calculate the number density of different species. The equilibrium composition of the gas mixture with a carbonic–phenolic injection consists of 21 chemical species (H_2, H, H^+, H^-, e^-, He^-, He^{2+}, C, C_2, C_3, C^+, C_2H, C_3H, C_4H, C_2H_2, O, O_2, O^+, CO, and CO_2). The equilibrium composition is determined by a free energy minimization calculation as developed in ref. [33].

Thermodynamic and transport properties

Thermodynamic properties for specific heat, enthalpy, and free energy, and transport properties for viscosity and thermal conductivity are required for each species considered in the shock-layer gas. Values for the thermodynamic and transport properties are obtained by using polynomial curve fits. For the solution with ablation injection, the mixture viscosity is calculated by using the semiempirical formula of Wilke [34] while the Lewis and Prandtl numbers are set equal to 1.1 and 0.64, respectively [35]. For the solutions without injection, the mixture transport properties for viscosity and Prandtl number are calculated using the correlations of Zoby *et al.* [36] and the Lewis number is assumed to be 1.1.

Entry trajectory and freestream conditions

The entry trajectories and freestream conditions used in this study are given in Tables 1 and 2. Trajectories I and II are applicable to both the 35° hyperboloid and 45° sphere cone, since both configurations have the same drag coefficient and the same base radius. Trajectory I represents the entry conditions resulting from the SO2P mission study [1] with the recommended nominal composition of Saturn's atmosphere as 89% H_2 and 11% He [16]. The entry is off the equatorial plane where the trajectory calculation is initiated (zero time) at an altitude of 450 km, a latitude of −3°, and a heading of S. 114.97°E. Trajectory II is for a relatively higher entry velocity. The entry conditions for this trajectory are for an equatorial entry where the trajectory calculations are initiated at an altitude of 1000 km. Further information on trajectories I and II is available in refs. [1, 8].

METHOD OF SOLUTION

A numerical procedure for solving the viscous shock-layer equations for stagnation and downstream regions is given by Davis [23]. Moss applied this method of solution to reacting multicomponent mixtures in refs. [11, 15]. A modified form of this procedure was used by Tiwari and Szema to investigate the effects of nonequilibrium chemistry for Jovian entry conditions [2]. The solution procedure used in this study is

Table 1. Altitude and freestream conditions: trajectory I

Time (s)	Altitudes (km)	ρ_∞ (kg m^{-3})	p_∞ (N m^{-2})	T (K)	V_∞ (km s^{-1})	Ma	Re
13	270.62	4.237E−5	14.287	91.40	27.952	40.537	8.107E+4
15	243.44	1.026E−4	33.591	88.78	27.676	40.726	1.980E+5
16§	236.70	1.290E−4	41.850	88.10	27.560	40.829	2.489E+5
16.75‡	220.02	2.259E−4	72.112	86.55	27.129	40.434	4.346E+5
17.75	206.93	3.526E−4	110.95	85.30	26.580	39.904	6.710E+5
19†	191.06	6.162E−4	190.36	83.73	25.503	38.643	1.139E+6
21	167.57	1.428E−3	428.54	81.33	22.504	34.600	2.374E+6
24	139.78	3.974E−3	1148.41	78.33	15.346	24.042	4.616E+6
26	127.19	6.410E−3	1820.43	76.99	10.751	16.989	5.274E+6

† Peak q_c, ‡ peak equilibrium q_r, § peak nonequilibrium q_r.

Table 2. Altitude and freestream conditions: trajectory II

Time (s)	Altitude (km)	ρ_∞ (kg m^{-3})	p_∞ (N m^{-2})	T (K)	V_∞ (km s^{-1})	Ma	Re
44	308.94	1.266E−5	4.449	95.28	32.116	45.620	2.709E+4
47	263.01	5.421E−5	18.132	90.66	31.893	46.442	1.190E+5
49	232.79	1.469E−4	47.542	87.76	31.401	46.475	3.241E+5
50.5§	210.64	3.099E−4	97.944	85.66	30.557	45.777	6.762E+5
51.75‡	192.83	5.790E−4	179.211	83.91	29.261	44.291	1.266E+6
52.5†	182.61	8.296E−4	253.752	82.91	28.103	42.792	1.700E+6
54	163.72	1.645E−3	490.985	80.91	24.739	38.135	3.016E+6
55	152.68	2.466E−3	725.114	79.71	21.781	33.825	4.019E+6
57	135.09	4.748E−3	1363.283	77.83	15.384	24.179	5.551E+6

† Peak q_c, ‡ peak equilibrium q_r, § peak nonequilibrium q_r.

identical to that given in refs. [2, 11] and, therefore, is not presented here.

RESULTS AND DISCUSSION

Results are presented for selected entry times (altitudes) shown in Tables 1 and 2 for trajectories I and II. Most of the results have been obtained for the 35° hyperboloid because of computational convenience. These are indicative also of the results for the 45° sphere cone because both configurations have the same drag coefficient and same base radius. Certain important results, however, are obtained also for the 45° sphere cone. Results are presented first to demonstrate the effects of nonequilibrium chemistry. Next, the solutions are presented (with and without ablation) for laminar flow. Finally, the results of turbulent flow are compared with results of laminar flow for the 45° sphere cone. It should be noted that, for clarity, the asterisks on the dimensional quantities have been left out in the tables and figures.

Nonequilibrium chemistry effects

Laminar solutions obtained for chemical equilibrium and nonequilibrium conditions are presented here to demonstrate the effects of nonequilibrium chemistry on the heating rates of the 35° hyperboloid in absence of mass injection. Equilibrium solutions have been obtained by employing two different radiation models and equations of state. In the first method, the exact equation of state, equation (10), and detailed radiation code RAD are used and the solutions are called equilibrium (exact). In the second method, the approximate equation of state, equation (11), and 58-step radiation model are employed and the solutions are designated as equilibrium (approximate). The noncquilibrium solutions are based on the exact equation of state, equation (12), and the 58-step radiation model.

Equilibrium and nonequilibrium stagnation-point convective and radiative heating rates are shown, as a function of entry altitudes (times), in Figs. 2 and 3 for trajectories I and II, respectively. The results clearly show that while nonequilibrium chemistry lowers the convective heating rates, it increases the rate of radiative heating considerably. This is noted especially in the range of entry times (altitudes) for peak heatings. This phenomena is a direct consequence of an entirely different nonequilibrium temperature distribution in the shock-layer gas [2]. The rate of radiative transfer in the shock layer depends strongly on the nonequilibrium species concentration and an effective electronic temperature. This, in turn, influences the rate of nonequilibrium convective energy transfer in the shock-layer gas. The equilibrium heating rates based on the exact equation of state are seen to be higher than those based on the approximate equation of state; the differences are found to be larger for conditions near peak convective heatings. The radiative heating rates are seen to be less sensitive to the equation of state used. It should be noted that while the equilibrium and nonequilibrium peak heating time (altitude) is the same for convective heating, for radiative heating the nonequilibrium peak occurs at an earlier time than the equilibrium peak. This phenomena was observed also for the Galileo probe entry heating [2].

It is evident from Fig. 2 that the peak convective heating occurs at an entry altitude $Z = 191.06$ km ($t = 19$ s) for trajectory I. For this altitude, the extent of peak convective heating is found to be about 35, 31, and 27 MW m^{-2} for equilibrium (exact), equilibrium (approximate), and nonequilibrium cases, respectively. For this trajectory, the peak equilibrium radiative heating (about 2.3 MW m^{-2}) occurs at $Z = 220.02$ km ($t = 16.75$ s) and peak nonequilibrium radiative heating (about 6.5 MW m^{-2}) occurs at $Z = 236.70$ km ($t \sim 16$ s). For this trajectory, therefore, the stagnation-point radiative heating is considerably lower than convective heating. For higher entry altitudes, however, the nonequilibrium radiative heating can be about 20% of the corresponding convective heating.

For trajectory II, the peak convective heating occurs at $Z = 182.61$ km ($t = 52.5$ s) and its magnitude is found to be about 63, 49, and 45 MW m^{-2} for equilibrium (exact), equilibrium (approximate), and nonequilibrium conditions, respectively. It is noted that nonequilibrium radiative heating dominates the stagnation-point heating at higher altitudes (early

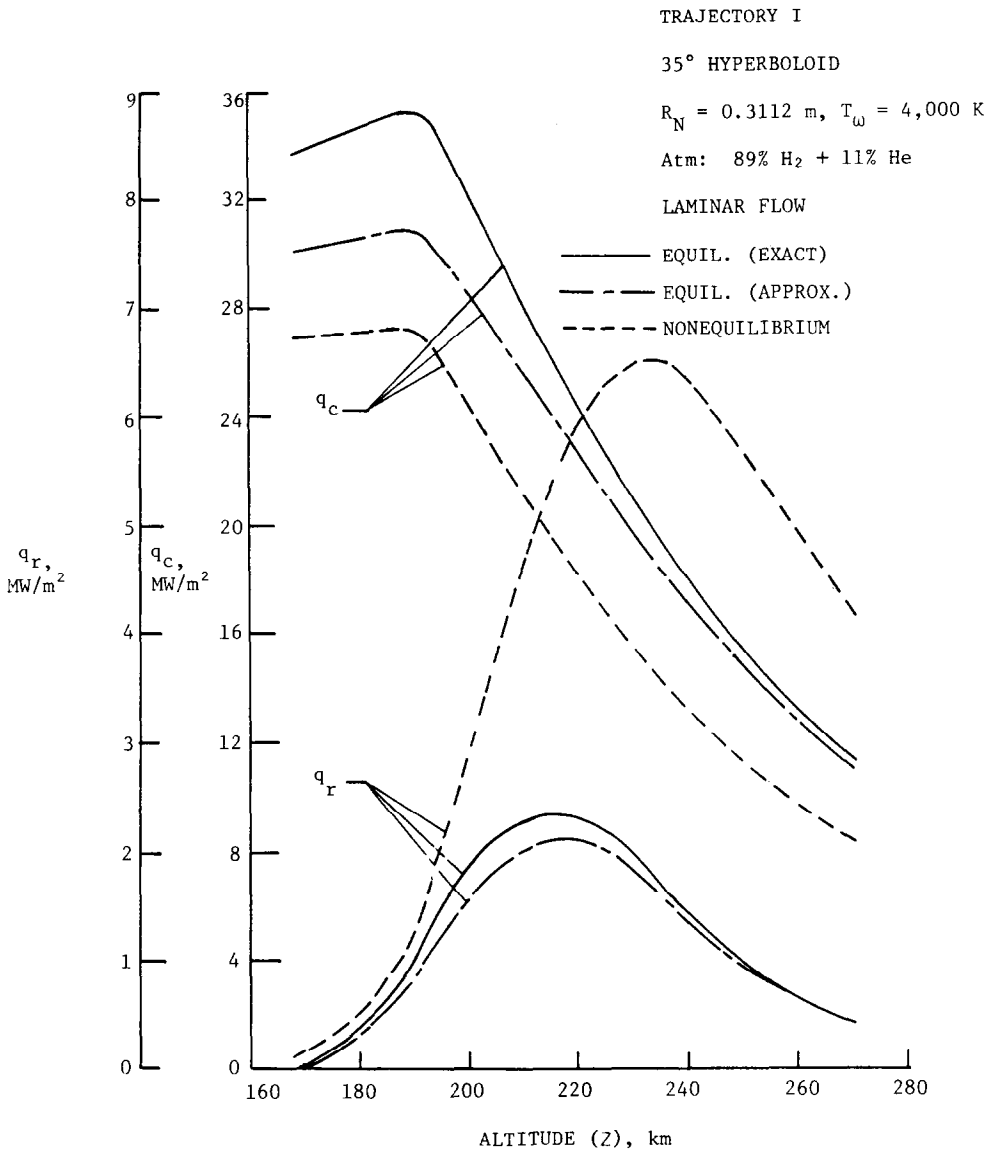

FIG. 2. Stagnation-point heating rate for nominal Saturn entry conditions, trajectory I, $q = q_w$, $\dot{m} = 0$.

times). The nonequilibrium peak radiative heating (about 88 MW m^{-2}) occurs at $Z = 210.64$ km ($t = 50.5$ s), whereas the equilibrium peak radiative heating (about 40 MW m^{-2}) occurs at $Z = 192.83$ km ($t = 51.75$ s). For this high speed entry trajectory, the stagnation-point radiative heating is found to be of the same order as the convective heating.

The shock-layer temperature variations are shown in Fig. 4 for trajectory I for the peak nonequilibrium radiative heating time. Results for other cases are available in ref. [10]. Equilibrium, as well as nonequilibrium results are presented for three different body locations ($\xi = 0$, 0.5, and 1.0). The equilibrium results based on exact and approximate equations of state are seen to follow the same general trend; however, the values are slightly different. The results clearly show that, just behind the shock, the nonequilibrium temperatures are much higher than the equilibrium temperatures. In the stagnation region (i.e. in the vicinity of $\xi = 0$–0.5), the nonequilibrium temperatures, in general, are higher than the equilibrium values. This is because relatively higher radiative energy transfer occurs (because of higher shock temperatures) toward the body in the stagnation region under nonequilibrium conditions [2, 10]. The reverse trend, however, is observed in the downstream region. This is due to the competing process of radiative energy transfer from the shock-layer gas toward the body and shock (i.e. toward the freestream) in the stagnation and downstream regions.

The heating rates along the forebody of the entry probe are shown in Figs. 5 and 6 for peak-heating freestream conditions of trajectories I and II, respectively. Equilibrium results indicate that convect-

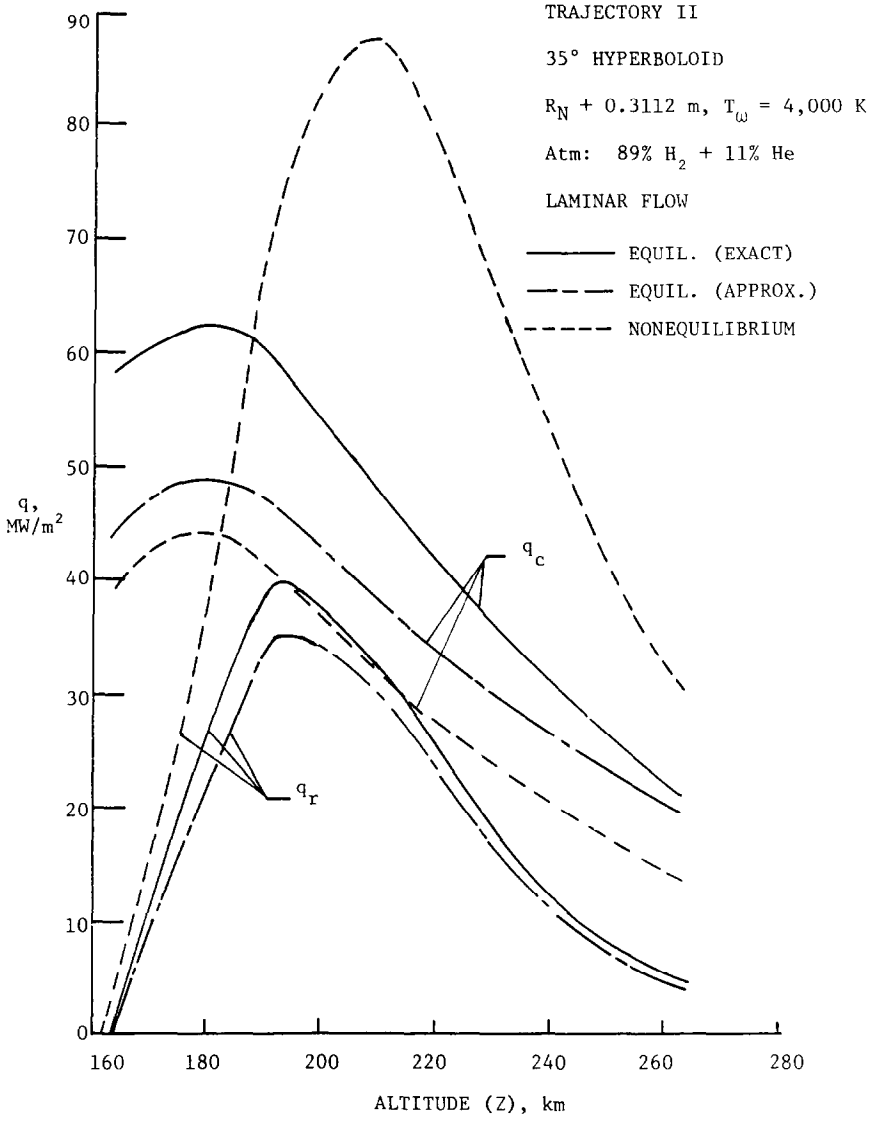

FIG. 3. Stagnation-point heating rate for nominal Saturn entry conditions, trajectory II, $q = q_w$, $\dot{m} = 0$.

ive heating is considerably higher than the radiative heating for all entry conditions. On this basis, therefore, it may be concluded that the dominant mode of heat transfer to the entry body is the convective heat transfer. This conclusion, however, cannot be derived on the basis of nonequilibrium results. Some general comments, however, can be made regarding all results before discussing specific results for each trajectory. In all cases, the radiative heating is seen to be important in the stagnation region. In this region, the nonequilibrium radiative heating rates are significantly higher than the equilibrium values. Both equilibrium and nonequilibrium rates are seen to decrease rapidly away from the stagnation point. This is a direct consequence of the temperature distribution in the shock layer (see Fig. 4). Convective heating rates, on the other hand, are not influenced dramatically due to the nonequilibrium conditions. This is because convective heat transfer essentially is a boundary-layer phenomenon and is greatly influenced by the temperature distribution in the vicinity of the body. The difference between equilibrium and nonequilibrium temperatures near the body is relatively small. The convective rates are seen to decrease slowly away from the stagnation point in comparison to the radiative heating rates. For the body locations greater than $\xi = 1.0$, the nonequilibrium results are seen to approach the equilibrium values in all cases.

For trajectory I, the heating rates along the body are shown in Fig. 5 for entry conditions at $Z = 236.70$ km ($t \sim 16$ s, the time for the peak nonequilibrium radiative heating). It is noted that the equilibrium results based on the approximate equations of state are significantly different than those of the exact equation of state; the differences are larger for convective heating than for radiative heating. The radiative heating is

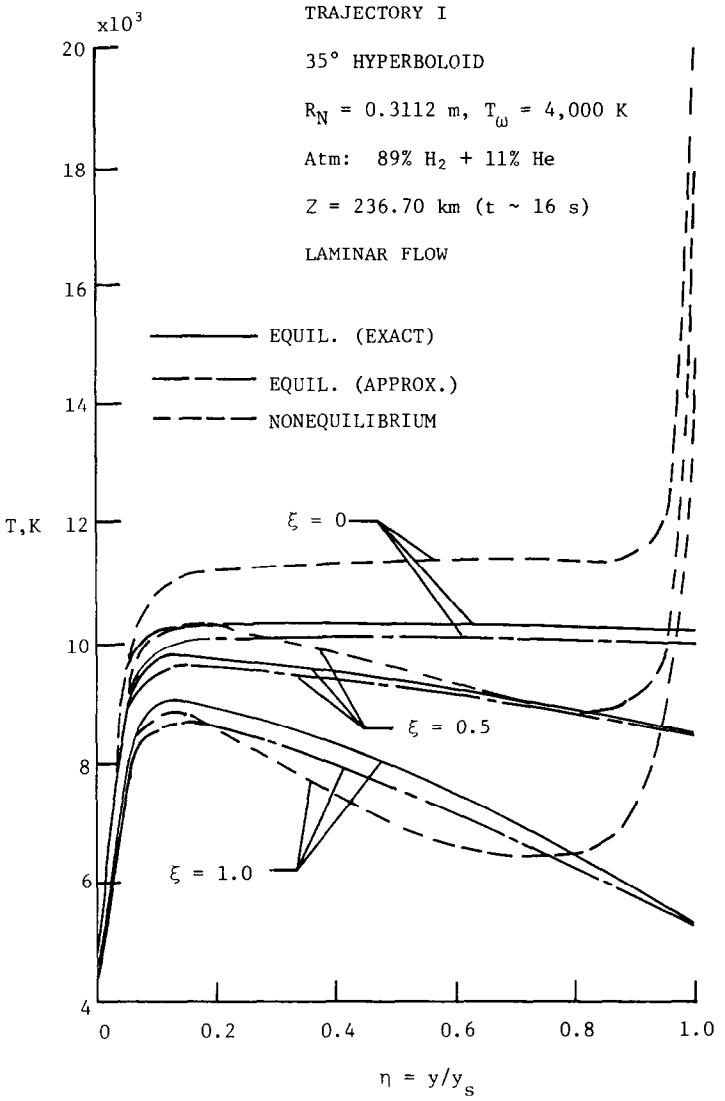

FIG. 4. Shock-layer temperature variation, trajectory I, $t \sim 16$ s, $\dot{m} = 0$.

seen to be important only in the stagnation region ($\xi = 0$–1.0). In the vicinity of the stagnation point, the nonequilibrium radiative heating reaches up to 25% of the convective heating but is negligible in the downstream regions. The results clearly show that the entry heating for this trajectory is dominated by the convective heating.

The heating rates along the body are shown in Fig. 6 for trajectory II. The equilibrium (exact) and equilibrium (approximate) results are seen to differ significantly only near the stagnation point. The results, in general, show that for this trajectory the radiative heating can be as important as the convective heating. Specific results presented in Fig. 6(a), for entry conditions at $Z = 182.61$ km, show that convective heating rates are higher than radiative heating rates. For this case, the convective heating load (i.e. the convective power) to the entry body will certainly be greater than the radiative heating load because of the larger surface area associated with the convective heating. The story is somewhat similar for the results presented in ref. [10] for conditions at $Z = 192.83$ km, except that the stagnation-point nonequilibrium radiative heating rate is now greater than the convective heating rate. For entry conditions at $Z = 210.64$ km, the results presented in Fig. 6(b) indicate that the convective and radiative heating load to the body will be approximately the same for nonequilibrium conditions.

The results presented in this section indicate the times (altitudes) for peak equilibrium and nonequilibrium heatings for trajectories I and II. The equilibrium results based on the approximate equation of state are found to differ significantly in the stagnation region. The effect of nonequilibrium chemistry is found to be important in the stagnation region. For the high

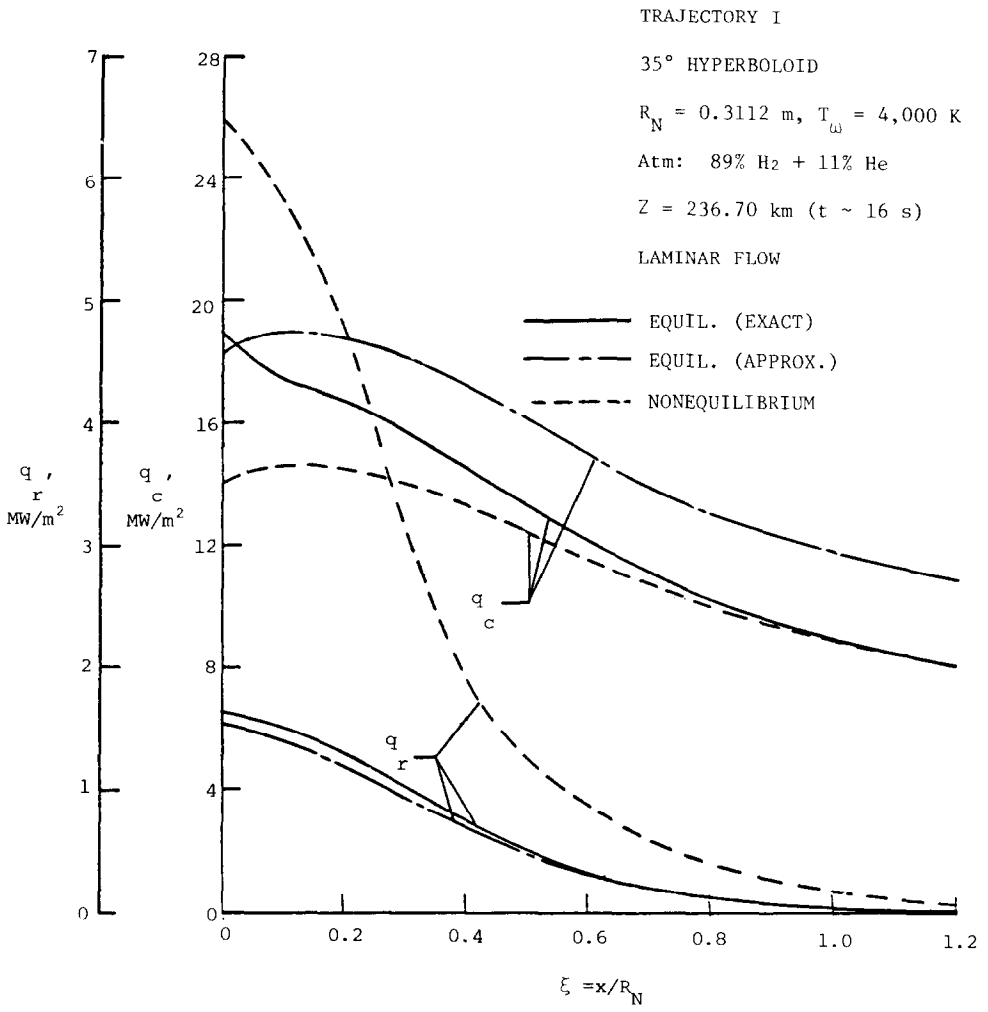

FIG. 5. Heating rates along the forebody, trajectory I, $t \sim 16$ s, $\dot{m} = 0$.

speed trajectory II, the radiative heating is found to be as important as the convective heating.

Coupled solutions: laminar flow

It is essential to provide adequate heat-shielding for thermal protection of the entry probe. This depends on effectiveness of the gaseous products of ablative material in reducing the surface heating rates. For the case of 35° hyperboloid and laminar flow, heating rates along the body (with and without ablation injection) have been calculated for the peak-heating entry conditions of trajectories I and II [10]. The results for trajectory II are shown in Fig. 7 for the peak convective heating entry conditions ($t = 52.5$ s); other results are available in ref. [10]. It is noted that while radiative heating is not effected significantly by the coupled mass injection, convective heating is reduced considerably in all cases. For the case of coupled injection, the stagnation region of the probe is dominated by the radiative heating, whereas the downstream region is dominated by the convective heating. An eight-fold reduction in convective heating is noted in the stagnation region. The results clearly show that heat-shield mass loss is dependent essentially on the extent of convective heating to the body.

Turbulent solutions

Turbulence can have a significant influence on the extent of heating of an entry probe. This is because turbulence significantly alters the composition, velocity, and temperature profiles in the shock layer [15]. For the 35° hyperboloid and the 45° sphere cone, heating rates along the body (with and without ablation injection) have been obtained for the peak-heating entry conditions of trajectories I and II [10]. According to ref. [15], instantaneous transition to turbulent flow at $X/R_N = 0.1$ is assumed. To demonstrate the influence of turbulence, results for entry time 51.75 s of trajectory II are shown in Fig. 8 for the 45° sphere cone. For the case with no mass injection, results presented in Fig. 8 (and ref. [10]) show that while turbulence has essentially no effect on the radiative heating, it increases

the convective heating rate substantially in the flank region of the probe. In the downstream regions, the turbulent convective rates are found to be twice the laminar heating rates. In the presence of mass injection, the results show that the radiative heating is slightly reduced in the stagnation region and increased in the flank region. However, as for laminar flow (Fig. 7), the convective heating is reduced considerably also for turbulent flow in the presence of mass injection. In this case also, the stagnation region is dominated by radiative heating and the downstream region by convective heating.

CONCLUDING REMARKS

The aerothermal environment of a Saturn entry probe has been investigated for currently specified nominal trajectories. The entry probe configurations considered are a 35° hyperboloid and a 45° sphere cone. The extent of convective and radiative heating rates to the entry probe are investigated under chemical equilibrium and nonequilibrium conditions for the case with no mass ablation. For this case solutions are obtained by using the exact and an approximate equations of state. Under assumption of chemical equilibrium, effects of coupled mass ablation are investigated for laminar and turbulent flows.

Results of the approximate equation of state are found to differ significantly from the results of the exact equation of state. Consequently, use of the approximate equation of state cannot be justified for the Saturn entry conditions. The effects of nonequilibrium chemistry, in general, are found to be important in the stagnation region; the effects are pronounced especially at earlier entry times (higher altitudes). While nonequilibrium chemistry causes a slight reduction in convective heating, it increases the radiative heating rate considerably in the stagnation region. Specific results show that it is possible to neglect the nonequilibrium effects for trajectory I since the extent of radiative heating is small for this trajectory. For the high speed entry trajectory II, however, the radiative heating is found to be as important as convective heating and nonequilibrium chemistry plays an important role in

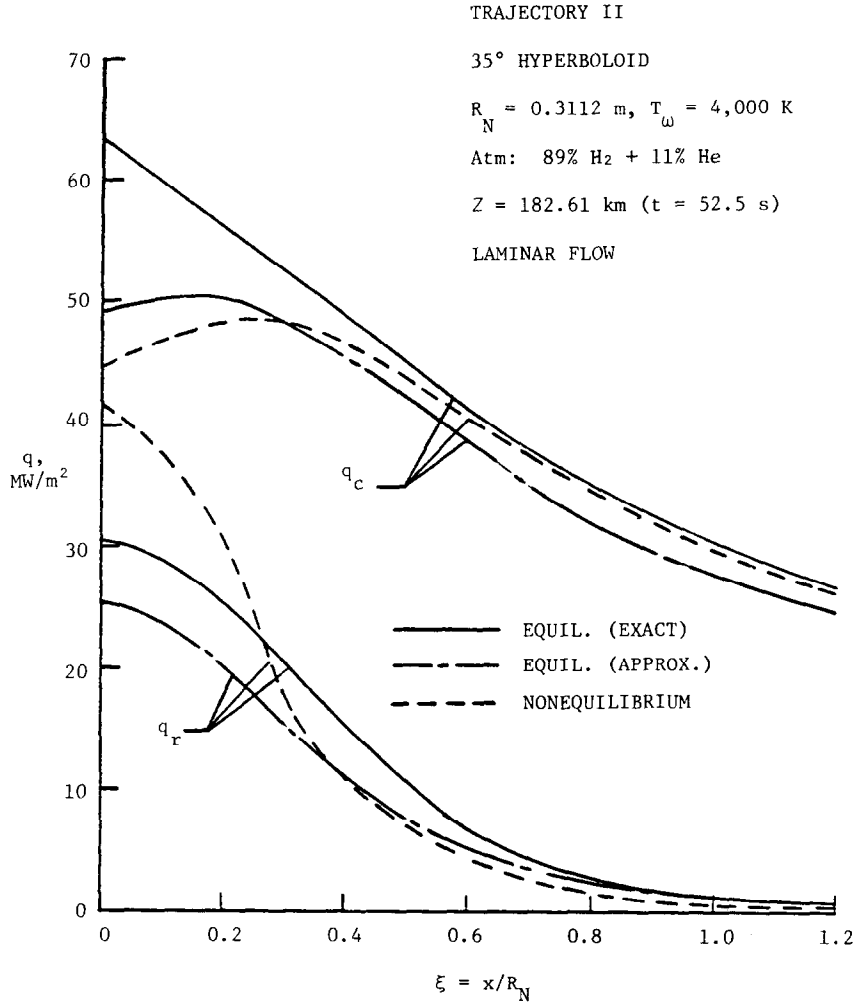

FIG. 6(a). Heating rates along the forebody, trajectory II, t = 52.5 s, $\dot{m} = 0$.

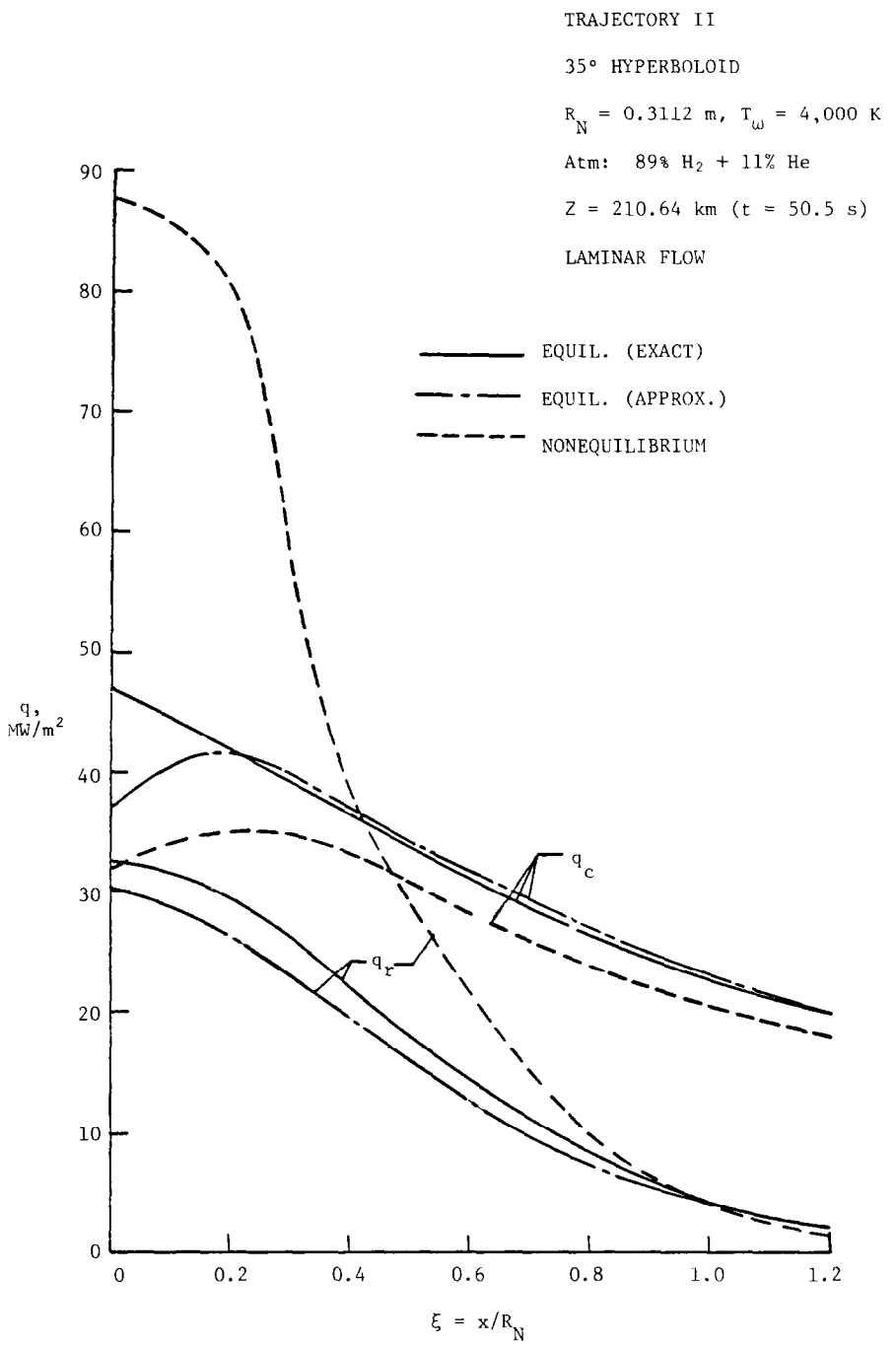

FIG. 6(b). Heating rates along the forebody, trajectory II, $t = 5.05$ s, $\dot{m} = 0$.

determining the total heating load of the entry body.

The radiative heating rate is not influenced significantly by the coupled mass injection but the convective heating is reduced considerably (especially in the stagnation region). Turbulence has very little effect on radiative heating but it increases the convective heating considerably. In the downstream region of the probe, the convective heating rates for turbulent flow are about twice the laminar flow values. Both the coupled mass injection and turbulent flow results clearly indicate that the stagnation region is dominated by the convective heating. However, the overall heat-shield mass loss is dependent essentially on the extent of convective heating of the body.

Acknowledgements—The authors express their sincere appreciations to S. N. Dwivedi, C. S. Vemuru, and H. Chow for providing some of the results presented in this study and to K. Sutton for originally suggesting the need for this investigation.

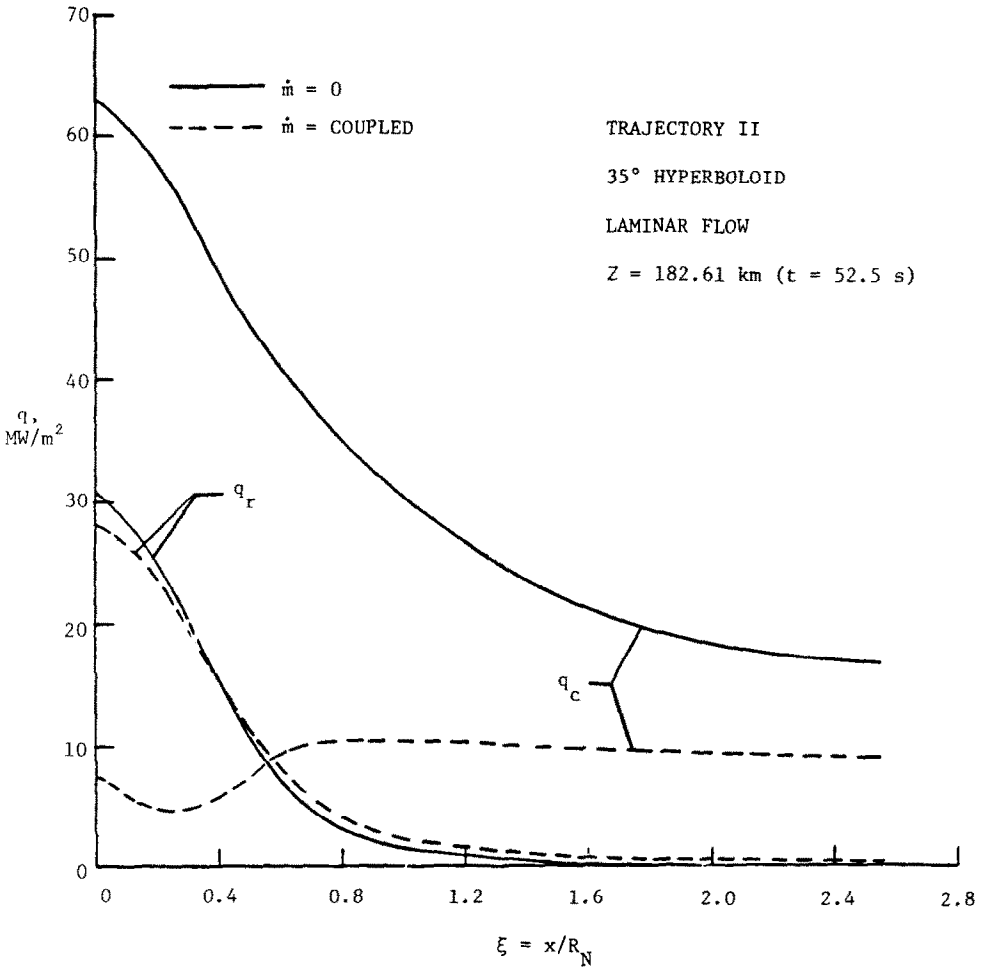

FIG. 7. Heating rates along the body with and without ablation injection, trajectory II, $t = 52.5$ s.

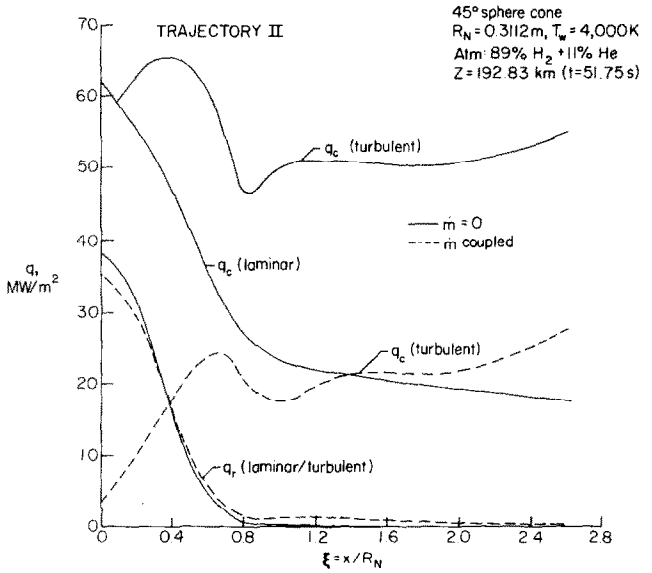

FIG. 8. Laminar and turbulent heating along the body (45° sphere cone), trajectory II, $t = 51.75$ s.

REFERENCES

1. J. L. Wright and A. R. Hibbs, Saturn orbital dual probe mission concept, NASA Report JPL 710-20, September (1978).
2. S. N. Tiwari and K. Y. Szema, Effects of precursor heating on radiative and chemically reacting viscous flow around a Jovian entry body, NASA CR-3186, October (1979); also, Influence of precursor heating on viscous flow around a Jovian entry body, NASA CR-3174, October (1979).
3. A. Kumar, K. Y. Szema and S. N. Tiwari, Nonequilibrium viscous flow over Jovian entry probes, AIAA Paper 79-1079, June (1970); also in *Progress in Astronautics and Aeronautics: Entry Heating and Thermal Protection* (edited by W. B. Olstad), Vol. 69, p. 104. AIAA, New York (1980).
4. W. E. Nicolet, J. T. Howe and S. A. Mezines, Outer planet probe entry thermal protection, Part I: aerothermodynamic environment, AIAA Paper 74-700, July (1974).
5. J. T. Howe, Hydrogen ionization in the shock layer for entry into the outer planets, *AIAA Jl* **12**, 875–876 (1974).
6. L. P. Leibowitz and T. Kuo, Outer planet entry nonequilibrium heating, AIAA Paper 75-1149, September (1975).
7. K. Sutton, Radiative heating about planet entry probes, AIAA Paper 75-185, January (1975).
8. E. V. Zoby and J. N. Moss, Preliminary thermal analysis for Saturn entry, AIAA Paper 80-0359, January (1980); also in *Progress in Astronautics and Aeronautics: Aerothermodynamics and Planetary Entry* (edited by A. L. Crosbie), Vol. 77, p. 374. AIAA, New York (1981).
9. E. V. Zoby, K. Sutton, W. B. Olstad and J. N. Moss, An approximate inviscid radiating flow field analysis for outer planet entry probes, AIAA Paper 78-189, January (1978); also in *Progress in Astronautics and Aeronautics: Outer Planet Entry Heating and Thermal Protection* (edited by R. Viskanta), Vol. 64, p. 42. AIAA, New York (1979).
10. S. N. Tiwari, Analysis of aerothermodynamic environment of a Saturn entry probe, School of Engineering, Old Dominion University, Norfolk, Virginia, Technical Report 82-8000, August (1983); also, Nonequilibrium chemistry effects for Saturn entry probe, NASA CR-NASI-15648-4, February (1980).
11. J. N. Moss, Reacting-viscous-shock-layer solutions with multicomponent diffusion and mass injection, NASA TR R-411, June (1974).
12. J. N. Moss, E. C. Anderson and C. W. Boltz, The effect of ablation injection on radiative and convective heating, NASA TM X-71976 (1974).
13. J. N. Moss, Viscous-shock-layer-solutions with radiation and ablation injection for Jovian entry, AIAA Paper 75-671, May (1975).
14. J. N. Moss, E. C. Anderson and C. W. Boltz, Aerothermal environment for Jovian entry probes, AIAA Paper 76-469, July (1976).
15. J. N. Moss, A study of the aerothermal entry environment for the Galileo probe, AIAA Paper 79-1081, June (1979).
16. Anon, *The Planet Saturn* (1970), NASA SP-8091, June (1972).
17. M. N. Rolin, R. I. Solukhin and F. B. Yurevich, Heat and mass transfer in an emitting compressed layer with reflection from the body surface and injection of ablation products, *Int. J. Heat Mass Transfer* **24**, 1771–1782 (1981).
18. R. B. Bird, W. E. Stewart and E. N. Lightfoot, *Transport Phenomenon*. Wiley, New York (1960).
19. W. H. Dorrance, *Viscous Hypersonic Flow*, McGraw-Hill, New York (1962).
20. W. G. Vincenti and C. H. Kruger, *Introduction to Physical Gas Dynamics*. Wiley, New York (1965).
21. E. C. Anderson, J. N. Moss and K. Sutton, Turbulent viscous-shock-layer solutions with strong vorticity interaction, AIAA Paper 76-120, January (1976); also, *J. Spacecraft Rockets* **14**, 32–37 (1977).
22. E. V. Zoby, P. A. Gnoffo and R. A. Graves, Correlations for determining thermodynamic properties of hydrogen–helium gas mixtures at temperatures from 7,000 to 35,000 K, NASA TN D-8262, August (1976).
23. R. T. Davis, Numerical solution of hypersonic viscous shock-layer equations, *AIAA Jl* **8**, 843–851 (1970).
24. S. N. Tiwari and S. V. Subramanian, Influence of nonequilibrium radiation and shape change on aerothermal environment of a Jovian entry body, NASA CR-3432, May (1981); also, S. V. Subramanian, Ph.D. Dissertation, School of Engineering, Old Dominion University, Norfolk, Virginia, March (1980).
25. G. H. Stickford, Total radiative intensity calculations for 100% H_2 and 87% H_2–13% He, *J. Quantve Spectros. Radiat. Transf.* **12**, 525–529 (1972).
26. W. E. Nicolet, Advanced methods for calculating radiation transport in ablation-product contaminated boundary layers, NASA CR-1656 (1970).
27. W. E. Nicolet, User's manual for the generalized radiation transfer code (RAD/EQUIL), NASA CR-116353, October (1969); also, User's manual for (RAD/EQUIL/1973), a general purpose radiation transport program, NASA CR-132470, November (1973).
28. K. Sutton and J. N. Moss, Radiation absorption by the C_2 band systems for Jupiter entry conditions, AIAA Paper 79-0033, January (1979).
29. J. N. Moss, J. J. Jones and A. L. Simmonds, Radiative flux penetration through a blown shock layer for Jupiter entry, AIAA Paper 78-908, May (1978); also in *Progress in Astronautics and Aeronautics: Outer Planet Entry Heating and Thermal Protection* (edited by R. Viskanta), Vol. 64, p. 22. AIAA, New York (1979).
30. F. H. Clauser, The turbulent boundary layer, in *Advances in Applied Mathematics* (edited by H. L. Dryden and Th. Von Karman), Vol. IV, Ch. 1. Academic Press, New York (1956).
31. P. S. Klebanoff, Characteristics of turbulence in a boundary layer with zero pressure gradient, NADA Rep. 1247 (1955), supersedes NASA TN 3178.
32. T. Cebeci, Behavior of turbulent flow near a porous wall with pressure gradient, *AIAA Jl* **8**, 2152–2156 (1970).
33. C. W. Stroud and K. L. Brinkley, Chemical equilibrium of ablation materials including condensed species, NASA TN D-5391 (1969).
34. C. R. Wilke, A viscosity equation for gas mixtures, *J. Chem. Phys.* **18**, 517–519 (1950).
35. N. T. Grier, Calculation of transport properties and heat-transfer parameters of dissociating hydrogen, NASA TN D-1406 (1962).
36. E. V. Zoby, R. A. Graves, J. N. Moss and A. Simmonds, Correlations for determining transport properties of hydrogen–helium gas mixtures at temperatures from 1000 to 25,000 K, AIAA Paper 79-0034, January (1979).

CHAUFFAGE CONVECTIF ET RADIATIF D'UNE SONDE D'ENTREE SUR SATURNE

Résumé—Le chauffage convectif et radiatif d'une sonde d'entrée sur Saturne est étudié en l'absence et en présence d'injection d'une masse ablative. L'écoulement dans la couche de choc est supposé axisymétrique, visqueux et en équilibre thermodynamique local. L'importance des effets de non-équilibre chimique à la fois pour les flux surfaciques radiatif et convectif est démontrée pour des conditions d'entrée prescrites. Des résultats montrent que le non-équilibre chimique peut influencer sensiblement le flux de chauffage radiatif sur les sondes d'entrée. Avec une injection mixte carbone–phénolique, les flux convectifs sont nettement réduits. La turbulence a un faible effet sur le chauffage radiatif mais elle accroît considérablement le chauffage convectif.

AUFHEIZUNG EINER SATURN-SONDE DURCH KONVEKTION UND STRAHLUNG

Zusammenfassung—Das Ausmaß der Erwärmung durch Konvektion und Strahlung für eine Sonde, die in die Saturn-Atmosphäre eintritt, wird für die Fälle mit und ohne Ablationskühlung untersucht. Die Strömung in der Stoßfrontschicht wird als achsensymmetrisch, zäh und im örtlichen thermodynamischen Gleichgewicht befindlich angenommen. Die Bedeutung von Einflüssen chemischen Nicht-Gleichgewichts auf die Erwärmung der Oberfläche durch Strahlung und Konvektion für vorgegebene Eintrittsbedingungen wird dargelegt. Die Ergebnisse zeigen, daß Abweichungen vom chemischen Gleichgewicht die Erwärmung der Sonden durch Strahlung stark beeinflussen können. Bei kombinierter Kohlenstoff–Phenol-Ablationskühlung wird die konvektive Erwärmung stark verringert. Die Turbulenz hat nur geringen Einfluß auf die Erwärmung durch Strahlung, erhöht aber merklich die Erwärmung durch Konvektion.

КОНВЕКТИВНЫЙ И ЛУЧИСТЫЙ НАГРЕВ ЗОНДА ПРИ ВХОДЕ В АТМОСФЕРУ САТУРНА

Аннотация—Проведено исследование степени конвективного и лучистого нагрева зонда при входе в атмосферу Сатурна в случаях без вдува и с вдувом массы для испарительного охлаждения. Предполагается, что поток в ударном слое осесимметричный, вязкий и локально равновесный. Показано существенное значение эффектов химического неравновесия как для лучистого, так и конвективного нагревов необдуваемой поверхности при заданных условиях входа зонда в атмосферу. Результаты показывают, что неравновесные химические процессы могут сильно влиять на интенсивность лучистого нагрева зондов. При вдуве смеси углерода с фенолом интенсивность конвективного нагрева существенно снижается. Турбулентность оказывает незначительное влияние на лучистый нагрев, но намного усиливает конвективный.